Chemical Engineering Journal 428 (2022) 132564

Contents lists available at ScienceDirect

Chemical Engineering Journal

journal homepage: www.elsevier.com/locate/cej

Modeling a biogas upgrading PSA unit with a sustainable activated carbon derived from pine sawdust. Sensitivity analysis on the adsorption of CO_2 and CH_4 mixtures

Inés Durán, Fernando Rubiera, Covadonga Pevida *

Instituto de Ciencia y Tecnología del Carbono, INCAR–CSIC, c/Francisco Pintado Fe, 26, 33011 Oviedo, Spain

ARTICLE INFO

Keywords:
Pine sawdust
Activated carbon
Biogas
Biomethane
Pressure Swing Adsorption
Modeling

ABSTRACT

Pressure Swing Adsorption (PSA) is one of the implemented technologies for removing carbon dioxide in biogas streams. Different adsorbents, mostly zeolite-based, and process configurations have been patented and commercially demonstrated. In this study, we have developed a numerical model to successfully describe the dynamic performance of biomass-derived activated carbon in biogas purification. It is the first step in designing a biomass-based carbon capture unit within the bioenergy and circular economy context.

Microporous activated carbon pellets prepared from pine sawdust by physical activation with CO_2 was the adsorbent material choice. The model was built with the fittings of single-component adsorption isotherms of CO_2 and CH_4 at different temperatures to the Langmuir-Freundlich model and the Ideal Adsorbed Solution Theory (IAST) to account for multicomponent adsorption. The kinetics of mass transfer in the solid phase was described by the Linear Driving Force model (LDF).

The dynamic simulations were performed with the aid of the commercial software Aspen Adsorption and experimental data previously obtained in the laboratory used for the model validation [1]. The model was applied to address the separation performance of a biogas upgrading biomass-based PSA process by running a parametric study to determine the influence of key performance parameters. The sensitivity analysis concluded that a single stage 4-step PSA can produce methane with a purity above 95% and a recovery of around 60% in a configuration with P/F ratios (quotients of molar flows of CH_4 in the purge and the feed streams) between 0.67 and 1 for an adsorption pressure of 3 bar.

1. Introduction

Rising interest in biomethane worldwide has recently surged as a renewable fuel for direct injection into the natural gas grid. The principal source of biomethane, besides the synthetic route, is biogas purification which separates CH_4 from CO_2 after prior removal of the other contaminants (e.g., H_2S, siloxanes).

The number of biomethane plants in Europe has considerably increased. According to the European Biomethane Map 2020 released by the European Biogas Association (EBA) and Gas Infrastructure Europe (GIE), there has been a 51% increase of biomethane plants in Europe over the past two years, from 483 in 2018 to 729 in 2020.

Different upgrading technologies are commercially available [2–5]. Adsorption processes like Pressure Swing Adsorption (PSA) have great potential for biogas upgrading to obtain biomethane [6]. Compared with other separation methods, PSA processes generally present lower energy requirements [7,8].

PSA processes driving force is the difference in the amount of gas adsorbed due to changing the pressure between the adsorption and regeneration steps. They were originally conceived by Skarstrom [9] in 1960 and have since become widely applied in gas separation applications like air separation, gas drying, hydrogen purification [10,11] and, more recently, CO_2 capture from flue gases [12]. Depending on the adsorbent material, gas mixture separation can be accomplished either by the difference in adsorption capacity (equilibrium separation) or by differences in the diffusion rates of molecules through the porous material (kinetic selectivity) [13,14]. Various types of adsorbents have been studied for biogas upgrading, including carbon molecular sieves (CMS) [15], activated carbons [16–21], zeolites [22–24] and metal–organic frameworks (MOFs) [25–28].

* Corresponding author.
E-mail address: cpevida@incar.csic.es (C. Pevida).

https://doi.org/10.1016/j.cej.2021.132564
Received 24 May 2021; Received in revised form 15 September 2021; Accepted 17 September 2021
Available online 22 September 2021

PSA process design is complex due to the multiple variables involved, the characteristic batch non-steady-state, and the infinite number of possible cycle configurations. Hence, mathematical modeling is a useful tool to reach optimal process configurations.

Modeling of PSA or VSA (Vacuum Swing Adsorption) biogas upgrading processes in fixed-beds has been ongoing research over the years [29] and remaining a hot topic for research to improve process performance and energy efficiency. Mathematical models for Skarstrom-type cycles include the fundamental steps: pressurization, adsorption, blowdown and purge [14]. Changes in the basic configuration were introduced by Kapoor et al. [30] with co-current depressurization and countercurrent blowdown steps, while Cavenati et al. [31] incorporated countercurrent pressurization and purge steps with a methane-rich product stream. The feasibility of configurations including additional stages to those in the Skarstrom cycle, such as pressure equalization steps, has been investigated for energy conservation [32–35]. Furthermore, Santos et al. [36] studied the effect of recycling contaminated streams from one column to another both in the purge and in pressure equalization steps. Shen et al. [37] simulated a dual Vacuum Pressure Swing Adsorption (VPSA) process with silica gel for removing CO_2 from biogas. A 9-step 4-bed VPSA process was deployed as a rectifying unit for CH_4 enrichment, and subsequently, an 8-step two-bed VPSA process was used as a stripping unit for CO_2 capture from the tail gas.

In this work, a biomass-based activated carbon was evaluated in a PSA process aiming for CO_2/CH_4 separation. Despite the PSA processes being commercial, most studies do not contemplate the use of activated carbons, much less biomass-derived, since, a priori, they do not present sufficiently high CO_2/CH_4 selectivity. However, these materials would offer side advantages such as reducing the environmental impact resulting from uncontrolled disposal residues, lower emissions during their production, and a unique opportunity to develop a circular economy and reach negative carbon emissions when compared to other CO_2 capture processes [38–41].

Aspen Adsorption™ software was used to model breakthrough curves data obtained experimentally. The validated mathematical model was then employed in the simulation of Skarstrom's basic four-step PSA process using pine sawdust activated carbon as adsorbent for the production of biomethane.

Several parametric analyses applied to PSA systems for biogas upgrading can be found in the literature. Bonnot et al. [42] evaluated the influence of composition, temperature, and purge on the performance of a PSA cycle for the separation of CO_2 and CH_4 using two activated carbons. A similar parametric study on a commercial activated carbon was carried out by Foeth et al. [43] to establish the effect that temperature, superficial velocity, and inlet partial pressure have on the breakthrough behavior of the adsorbates. A comparison of three adsorbents with different separation mechanisms (a MOF, zeolite 13X, and CMS-3 K) tested for a 2-bed 6-step modified Skarstrom cycle has been reported [44]. The key factors chosen in this study were the adsorption and desorption pressures and the P/F ratio, defined as the ratio between the molar flows of CH_4 in the purge and the feed streams. These studies proved beneficial to determine the optimum values of process parameters to maximize product purity and recovery.

Thus, the last section of this paper addresses a parametric analysis to establish the influence of different variables on the process performance: adsorption and regeneration pressure, purge flow rate etc.

2. Materials and methods

Key input variables for the design of adsorption-based separation processes include multicomponent gas adsorption equilibria, kinetics, and heat balance. The three components must be known accurately under all the conditions encountered during the cyclic process.

This section will analyze the experimental data gathered to build the specific model for the biogas upgrading process of interest.

Table 1
Fittings of the CO_2 and CH_4 adsorption isotherms to the Langmuir-Freundlich model.

	CO_2	CH_4
***IP1* (kmol/kg)**	6.107×10^{-3}	5.864×10^{-3}
***IP2* (1/bar)**	6.312×10^{-4}	6.030×10^{-4}
***IP3* (−)**	7.315×10^{-1}	7.831×10^{-1}
***IP4* (K)**	2.108×10^{3}	1.864×10^{3}
***IP5* (1/bar)**	8.507×10^{-4}	7.688×10^{-4}
***IP6* (K)**	1.982×10^{3}	1.847×10^{3}
RSS	7.29×10^{-3}	4.54×10^{-3}

2.1. Adsorption equilibrium data

Pine sawdust activated carbon was used as an adsorbent. They were produced in our laboratory by physical activation with CO_2 of pine sawdust pellets. The comprehensive characterization was reported elsewhere [45].

When modeling gas adsorption-based separation, it is mandatory to select models (theoretical or empirical) to account for pure and multicomponent gas adsorption equilibria. Adsorption isotherms of CO_2 and CH_4 at 30, 50, and 70 °C up to 10 bar were determined in a high-pressure Rubotherm-VTI magnetic suspension balance (Fig. S1 in the Supplementary Materials). The pure component adsorption equilibrium data were fitted to the Langmuir-Freundlich isotherm model. The form of the isotherm equation in Aspen Adsorption is as follows:

$$w_i = \frac{IP_1 IP_2 P_i^{IP_3} e^{IP_4/T_s}}{1 + IP_5 P_i^{IP_3} e^{IP_6/T_s}} \quad (1)$$

where w_i is the equilibrium loading of component i (kmol/kg- adsorbent), P_i is the equilibrium partial pressure of component i (bar), and Ts is the temperature (K). The fittings and units of the different isotherm parameters (IP_i) are summarized in Table 1. Commonly, helium is assumed not to adsorb on the activated carbon.

The Residual Sum of Squares (RSS) states the deviation between the experimental results and the values predicted by the isotherm models. It was calculated for each gas component as follows:

$$RSS(\%) = \sqrt{\frac{\sum_{i=1}^{n} (q_{\exp} - q_{model})_i^2}{n-1}} x100 \quad (2)$$

where $q_{\exp}$ and q_{model} refer to the measured and model predicted values of the amount adsorbed, respectively, and n represents the number of experimental data points fitted for each experiment. The model accurately represents the adsorption of CO_2 and CH_4 at the three temperatures as shown in the minimal RSS values and the fittings plotted in Fig. S1 (Supplementary Material).

To model multicomponent gas adsorption, the Ideal Adsorbed Solution Theory (IAST) was applied using the fittings for the individual components (details included in the Supplementary Material). This model accounts for the competitive adsorption of CO_2 and CH_4 on the activated carbon that is observed during the experiments.

Table 2
Adsorbent bed characteristics.

Parameter	
Height of adsorbent layer, h_b (cm)	11.85
Internal diameter of adsorbent layer, d_b (cm)	1.3
Inter-particle voidage, ε_i (−)	0.581
Intra-particle voidage, ε_p (−)	0.681
Bulk solid density of adsorbent (kg/m^3)	255.7
Adsorbent particle radius, rp (mm)	1.48
Adsorbent shape factor (−)	0.91
Void volume before the column (cm^3)	4.34
Void volume after the column (cm^3)	10.4

Table 3
Experimental conditions of the breakthrough curve experiments.

	Pressure (bar)	Temperature (°C)	Total feed flow rate (cm^3/min)	Feed composition (vol. %)	
				CO_2	CH_4
Exp 1	1.2	30	30	50	50
Exp 2	1.2	30	15	50	50
Exp 3	1.2	30	50	50	50
Exp 4	1.2	30	30	65	35
Exp 5	1.2	30	30	30	70
Exp 6	3	30	30	50	50
Exp 7	5	30	30	50	50
Exp 8	10	30	30	50	50

2.2. Breakthrough tests in a fixed-bed set-up

A single fixed-bed unit packed with approximately 4 g of pellets of the activated carbon (length: 11.85 cm, diameter: 1.3 cm) has been used to conduct cyclic adsorption–desorption experiments. A full description of the experimental set-up was reported elsewhere [1]. The main characteristics of the adsorbent bed are listed in Table 2.

Breakthrough adsorption experiments were conducted feeding CO_2/CH_4 binary gas mixtures representative of biogas streams to the set-up during the adsorption step, and helium was the inert gas carrier to assist desorption.

Firstly, the adsorbent bed followed a conditioning step by flowing 50 mL/min of He for 60 min at 180 °C and atmospheric pressure. Then, the bed cooled down, and the pressure raised, when required, to meet the adsorption conditions during a pre-conditioning step for 20 min, flowing 50 mL/min of He through the system. Afterward, the adsorption step began feeding the binary gas mixture to the column for 60 min to assure complete saturation of the adsorbent bed. An adsorption temperature of 30 °C was kept constant, and the adsorption pressure ranged between atmospheric pressure and 10 bar. Finally, the regeneration step was accomplished by pressure and temperature swing where the pressure dropped down to 1.2 bar and the temperature raised to 180 °C, until the bed was fully regenerated. Table 3 summarizes the experimental conditions for the adsorption step in each case study.

3. Modeling dynamic breakthrough experiments

The data from the breakthrough curves performed in the fixed-bed set-up at laboratory scale [1] were used in the validation of the dynamic model of these experiments.

3.1. Numerical model

A numerical model was developed in Aspen Adsorption™ to predict the breakthrough behavior of biogas CH_4/CO_2 mixtures in a fixed-bed packed with the activated carbon. The model consists of a combination of the mass, momentum, and energy conservation equations, adsorption equilibrium and kinetics models, as well as initial and boundary conditions. The first-order upwind differencing scheme (UDS1) with 50 nodes was selected as the method for spatial discretization.

The following assumptions were taken into consideration:

- The mass, energy, and momentum gradients are considered only in the axial direction.
- The bed operates under isothermal conditions.
- Void and bed density are constant along the column.
- A linear driving force (LDF) model is used to describe the mass transfer resistance.

$$\frac{\partial q_i}{\partial t} = MTC_{LDF,i}\left(q_i^* - q_i\right) \tag{3}$$

where q_i and q_i^* are the amount of the component i adsorbed at a given time and at equilibrium, respectively, and $MTC_{LDF,i}$ refers to the mass transfer coefficient.

The adsorbent bed characteristics summarized in Table 2 were input data in the simulation.

The LDF model describes the kinetics of the process using a lumped-up mass-transfer coefficient. It was determined by fitting the model to the experimental data at each condition. The Residual Sum of Squares (RSS) that accounts for the deviation between the experimental ($_{exp}$) and model predicted values ($_{model}$) was evaluated using an expression similar to equation (2) but changing the amount adsorbed (q) with molar fraction (y), to find the optimal value.

As reported by Shafeeyan et al. in a comprehensive review [29], the LDF approximation is the most widely used to model the mass transfer rate. Several modifications have been studied over the years. A bidisperse double LDF model has also been proposed to account for both macropore and micropore diffusion [46,47]. Even though the assumption of a constant LDF mass transfer coefficient is generally accepted and shows good accuracy, non-constant LDF coefficients have also been explored. Kapoor and Yang [30] used the LDF model approach with a cycle time-dependent. Kim et al. [32] predicted the adsorption dynamics of a carbon molecular sieve-based PSA process using a modified LDF model with concentration-dependent diffusivity due to the strong dependency of the sorption rate on the concentration. A variable mass transfer model was introduced by Park et al. [48] as a function of the effective intra-particle porosity, pressure, temperature, and adsorbate concentration. It provided an accurate estimate of the mass transfer rate for a wide range of adsorbate compositions for a CO_2/N_2 flue gas mixture fed to a Zeolite 13X - packed fixed-bed.

A LDF mass transfer relationship with pressure-dependent coefficients has also been evaluated in the literature [49,50]. Raghavan et al. [51] attributed the goodness of fit between the experimental data

Table 4
Estimated values for the parameters of the pressure-dependent MTC model.

	MTC CO_2 (1/s)	MTC CH_4 (1/s)	MTC He (1/s)	k_{0P} CO_2 (bar/s)	k_{0P} CH_4 (bar/s)	k_{0P} He (bar/s)	E_{act} CO_2 (kJ/mol)	E_{act} CH_4 (kJ/mol)	E_{act} He (kJ/mol)
Exp 1	0.15	1.0	1.0	21.0	63.4	1.0	12.0	10.0	1.0
Exp 2	0.05	1.0	1.0	7.0	63.4	1.0	12.0	10.0	1.0
Exp 3	0.2	1.0	1.0	28.1	63.4	1.0	12.0	10.0	1.0
Exp 4	0.3	1.0	1.0	42.1	63.4	1.0	12.0	10.0	1.0
Exp 5	0.1	1.0	1.0	14.0	63.4	1.0	12.0	10.0	1.0
Exp 6	0.03	1.0	1.0	10.5	158.6	1.0	12.0	10.0	1.0
Exp 7	0.005	1.0	1.0	2.9	264.3	1.0	12.0	10.0	1.0
Exp 8	0.0016	1.0	1.0	1.7	528.6	1.0	12.0	10.0	1.0

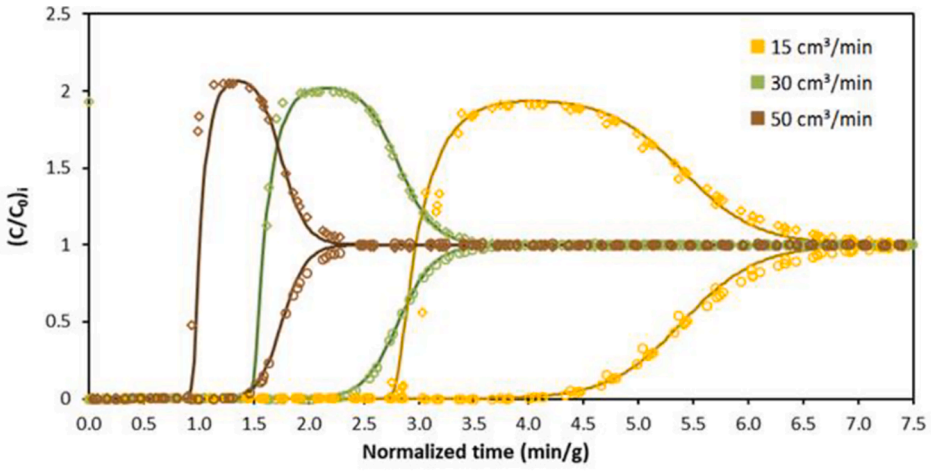

(a)

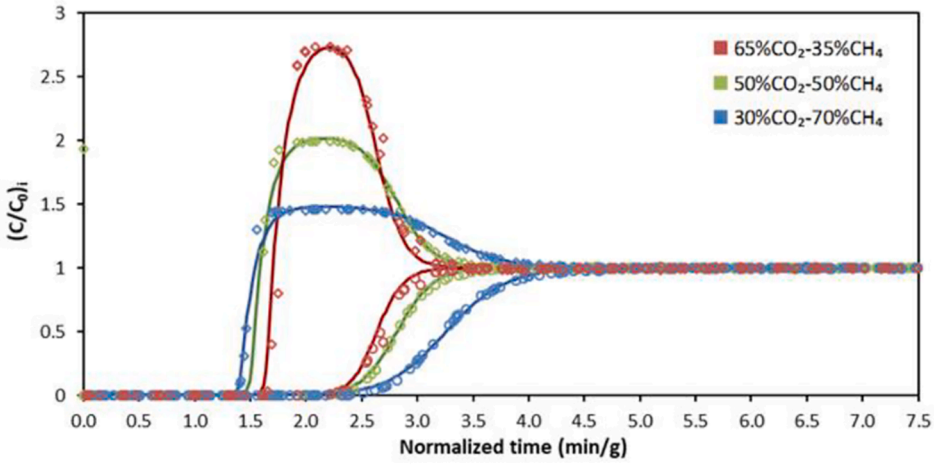

(b)

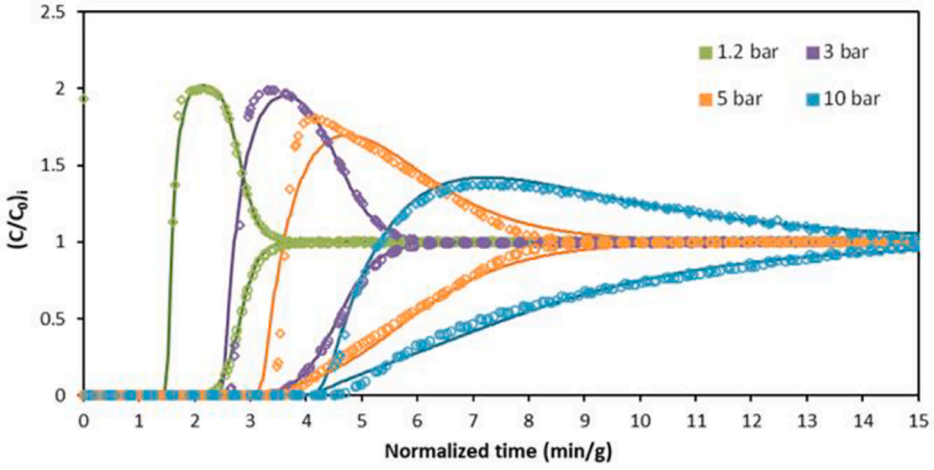

(c)

Fig. 1. Experimental (symbols) and simulated (solid lines) breakthrough curves of CH_4 (diamond) and CO_2 (circle) for: (a) different total feed flows (Experiments 1, 2 and 3); (b) different concentrations in the feed (Experiments 1, 4 and 5); (c) different total pressures (Experiments 1, 6, 7 and 8).

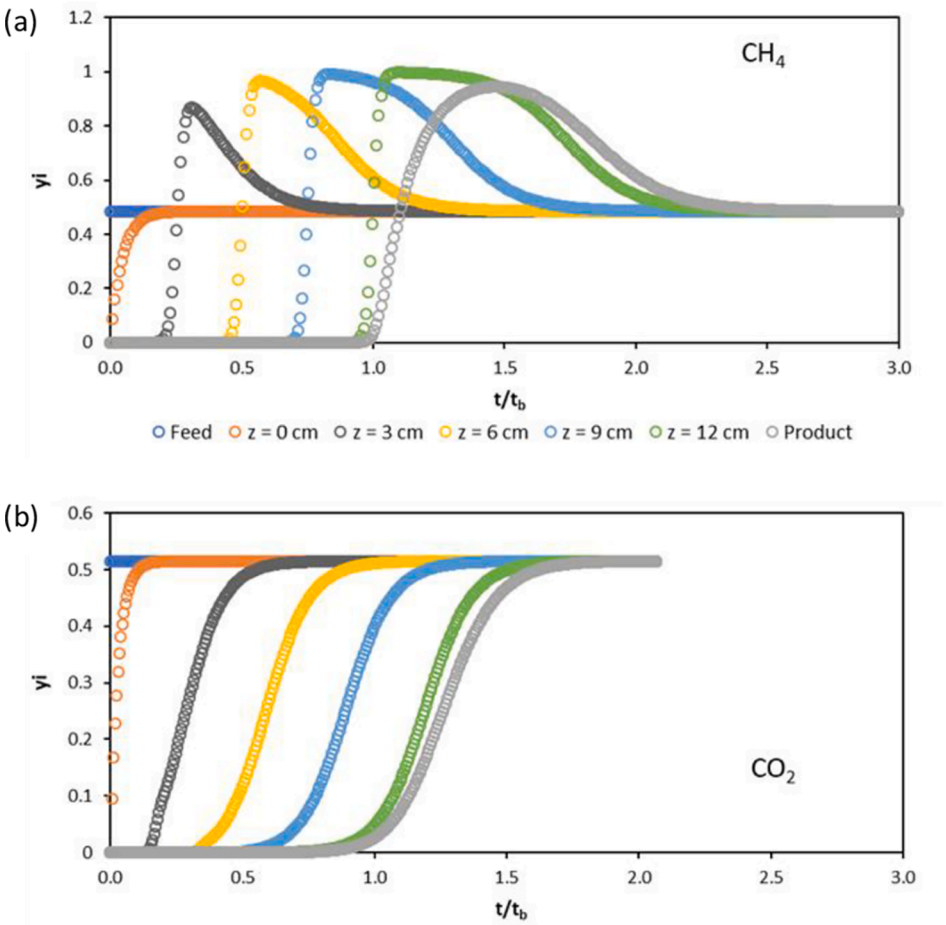

Fig. 2. Simulations of the molar fraction profiles of CH_4 (a) and CO_2 (b) at different locations in the bed for the experiment at 3 bar *vs.* a dimensionless time defined relative to the respective breakthrough time.

and the model to the mass transfer coefficient varying inversely with pressure. In Aspen Adsorption™, the mass transfer coefficient can be expressed with the following equation to account for the pressure effect:

$$MTC_i = \frac{k_{0P_i}}{P}\exp\left(\frac{-E_{acti}}{RT}\right) \quad (4)$$

where k_{0P} is the pre-exponential factor for pressure-dependent Arrhenius MTC model (in bar/s), and E_{act} is the activation energy factor for Arrhenius MTC model (in kJ/mol), for each gas component (i). As reported in the literature, the activation energy has been found experimentally to fall in the range of $Q/3 < E_{act} < Q$ [5230], where Q is the heat of adsorption. The heats of adsorption were estimated from the experimental data of the adsorption isotherms, obtained at different temperatures, using the Clausius-Clapeyron equation, resulting in values of 24 and 20 kJ/mol for CO_2 and CH_4, respectively.

Table 4 shows the values of the mass transfer coefficients estimated by adjusting the model simulation to match the slope of the gas components breakthrough curves at the different experimental conditions evaluated.

Besides, the pre-exponential k_{0P} factor for pressure-dependent Arrhenius MTC model was estimated assuming activation energy of about half the heat of adsorption. The optimum MTC values were finally selected based on purposely-conducted sensitivity analysis (see Figs. S2 and S3 in the Supplementary Material).

3.2. Model validation with experimental data

Breakthrough curves performed at a wide range of experimental conditions including different biogas compositions, total gas flow rates and adsorption pressures, under isothermal (30 °C) adsorption were analyzed (see [1] for further details about the experimental protocol). They intended to strengthen the dynamic model before applying it to the simulation and design of a PSA process for biogas upgrading.

The starting conditions in the simulation set the fixed-bed and void volume filled with He, at atmospheric pressure and 30 °C, to reproduce the experiments. A CO_2/CH_4 gas mixture fed the bed during the adsorption step that proceeded until reaching saturation ($(C/C_0)_i = 1$ for CO_2 and CH_4). The simulations of the breakthrough curves of CH_4 and CO_2 at different adsorption pressures (from 1.2 bar up to 10 bar) are shown in Fig. 1 plotted against a time normalized by the mass of adsorbent used for the breakthrough experiments.

There is a good agreement between the experimental and simulated breakthrough curves, as evidenced in Fig. 1. CH_4 exhibits the so-called roll-up, where methane concentration at the bed exit exceeds the inlet concentration. This is due to the preferential adsorption of CO_2 over CH_4 that displaces the previously adsorbed CH_4. The roll-up shape and intensity change with the adsorption conditions, and particularly at higher adsorption pressures. The model is capable of reproducing this effect quite accurately thanks to the Ideal Adsorbed Solution Theory (IAST), which accounts for the competitive adsorption of both gas components. It is important to recall that the experiments run at a constant adsorption temperature of 30 °C due to the experimental set-up incorporating a system to control the temperature of the adsorbent bed.

Fig. 2 shows the molar fraction profiles of CH_4 and CO_2 at different locations of the column for the experiment at 3 bar (Exp. 6): gas inlet to the adsorbent bed (z = 0 cm), at intermediate points of the bed at 3, 6,

Table 5
Adsorption capacities and breakthrough times estimated in the simulations.

	q CO_2 (mmol/g)		q CH_4 (mmol/g)		t_b CO_2 (min)	t_b CH_4 (min)	S CO_2/CH_4
Exp 1	1.97	(-9.4%)	0.60	(+13.7%)	9.5 (-0.3%)	5.9 (+6.6%)	3.27
Exp 2	1.90	(-13.9%)	0.63	(+11.7%)	18.2 (-0.5%)	11.1 (+1.6%)	3.01
Exp 3	2.01	(-10.8%)	0.59	(+6.4%)	5.9 (+4.3%)	3.7 (+4.0%)	3.43
Exp 4	2.32	(-11.9%)	0.41	(+9.7%)	9.3 (-0.2%)	6.4 (+3.5%)	5.62
Exp 5	1.41	(-9.1%)	0.90	(+3.0%)	10.2 (-3.6%)	6.1 (+9.2%)	1.56
Exp 6	3.11	(-9.3%)	1.02	(+5.0%)	14.5 (-1.6%)	10.0 (-2.6%)	3.05
Exp 7	3.90	(-12.5%)	1.40	(-1.6%)	14.7 (-5.4%)	12.5 (-2.0%)	2.79
Exp 8	5.32	(-15.8%)	2.18	(-9.6%)	17.6 (-9.4%)	17.2 (-0.2%)	2.44

and 9 cm from the gas inlet, and at the exit of the bed (z = 12 cm). Besides, the feed and product streams are also represented.

These profiles show how the gas components concentration evolves in the bed, and the dead volume of the set-up affects these profiles. The slope of the breakthrough curves changes as the gas components move through the column. At the bed inlet, the CO_2 advance-front curve (Fig. 2b) is steeper, but from a certain length of the bed, the slope remains constant. In Fig. 2a it can be observed that the shape of the methane roll-up varies considerably, becoming wider and higher as it flows along the bed. The difference between the shape of the roll-up just at the end of the bed and the product stream is due to the dead volume in the device softening effect.

Table 5 summarizes the CO_2 and CH_4 adsorption capacities (q_{CO2} and q_{CH4}), breakthrough times (t_b) and separation factor (S CO_2/CH_4) estimated for each simulation. The adsorption capacities were estimated following the graphical protocol of García et al. [53]. The ability of the activated carbon bed to separate CO_2 from CO_2/CH_4 mixtures was estimated with the separation factor as the quotient between qCO_2 and qCH_4. The deviations of the simulated values from the experimental data are reported between brackets.

The adsorption capacities increase with pressure, as expected. CO_2 and CH_4 uptakes calculated in the simulations match the experimental results. While the quantity of CO_2 adsorbed is slightly underestimated, at atmospheric pressure CH_4 uptake is overestimated by approximately the same extent. Particularly the experiment at 10 bar (Exp. 8) shows a considerable underestimation in the amount of adsorbed CH_4 predicted by the simulation.

Regarding the breakthrough times (time corresponding to C/C_0 = 0.05), the simulations accurately reproduce the experimental values for both CO_2 and CH_4. The only two cases where the deviation in the CO_2 breakthrough times is more substantial are the experiments at 5 and 10 bar (Exp. 7 and 8). The time elapsed between CH_4 and CO_2 breakthrough points to the separation capacity of the adsorbent bed. The largest gap in breakthrough times between both adsorbates was observed in the experiments at a pressure of 3 bar (Exp. 6) for selected gas composition and flow rate. Therefore, the enhanced effectiveness of the separation is expected at these conditions.

The divergence in the simulation when using a constant or a pressure-dependent Arrhenius MTC was also evaluated for both the adsorption and desorption steps. The regeneration was carried out by pressure and temperature swing, reducing the pressure to atmospheric and increasing the temperature to 180 °C. It was observed that when both the adsorption and desorption pressure kept at 1.2 bar (temperature swing solely), the simulation results in both cases, constant MTC or a pressure-dependent Arrhenius MTC, overlapped, as might be expected. However, in the cases where adsorption occurs at higher pressures, dissimilarities were observed in the simulations (see Fig. 3), and the significance of the pressure-dependent MTC turns apparent.

The choice of a constant or a pressure-dependent MTC turned out especially important at adsorption pressures of 5 and 10 bar. A constant MTC for the complete cycle (adsorption and desorption stages) results in a much slower rate of desorption of the gas components in the simulations compared to the experiments. In PSA cyclic processes, this can specifically affect the estimation of the product purity values. In the case of adsorptive separation at an adsorption pressure below 3 bar, the results would be very similar with both mass transfer coefficients.

4. Simulation of PSA cycles

Once validated with the experimental results, the dynamic model was the starting point in the design and optimization of the cyclic PSA process aiming to upgrade dry biogas. An approach based on a one-column scheme, considering the same dimensions as the experimental bed, was selected to carry out simplified simulations of PSA cycles. See the Supplementary Material for the flowsheet and numerical model equations.

A four-step single-bed PSA design was preset for the separation of CO_2 from CH_4 by adsorption on a bed with the activated carbon. It comprises the following steps:

(1) Pressurization: the column is pressurized using the feed mixture of CO_2/CH_4.
(2) Adsorption: the binary mixture feeds the adsorber, and a purified stream of the less selectively adsorbed gas component (i.e., CH_4) is produced.
(3) Blowdown: it is carried out counter-currently to the feed to maximize the product purity and prevent contamination with the raffinate accumulated at the exit of the bed.
(4) Purge with the product: the stream used in the purge step was pure methane. This step also proceeds counter-currently at low pressure.

Fig. 4 illustrates the schematic diagram of the cyclic configuration.

The temperature of the column was kept constant throughout the PSA cycle. Therefore, the simulations are considered isothermal. For the PSA cycles simulation, identical dead volumes before and after the column were considered (7.4 cm^3).

To assess the performance of the cycle configurations key parameters were estimated: product (CH_4) purity, recovery and productivity, and CO_2 purity and recovery. They are defined as follows:

$$CH_4\ purity = \frac{mol\ CH_4\ in\ raffinate}{total\ mol\ CH_4\ fed\ in\ cycle\ time} = \frac{\int_0^{t_A} F_{CH_4 out}\, dt}{\int_0^{t_A} F_{CH_4 out}\, dt + \int_{t_B}^{t_{Pu}} F_{CH_4 in}\, dt} \quad (5)$$

$$CH_4\ recovery = \frac{mol\ CH_4\ in\ raffinate}{mol\ CH_4 + mol\ CO_2\ in\ feed} = \frac{\int_{t_0}^{t_A} F_{CH_4 out}\, dt}{\int_0^{t_A} F_{CH_4 in}\, dt + \int_{t_B}^{t_{Pu}} F_{CH_4 in}\, dt} \quad (6)$$

$$CH_4\ productivity = \frac{mol\ CH_4\ in\ raffinate}{m_{adsorbent} \bullet t_{cycle}} = \frac{\int_{t_P}^{t_A} F_{CH_4 out}\, dt}{m_{adsorbent} \bullet t_{cycle}} \quad (7)$$

$$CO_2\ purity = \frac{mol\ CO_2\ in\ extract}{mol\ CH_4 + mol\ CO_2\ in\ extract} = \frac{\int_{t_A}^{t_B} F_{CO_2 out}\, dt}{\int_{t_A}^{t_B} F_{CH_4 out}\, dt + \int_{t_A}^{t_B} F_{CO_2 out}\, dt} \quad (8)$$

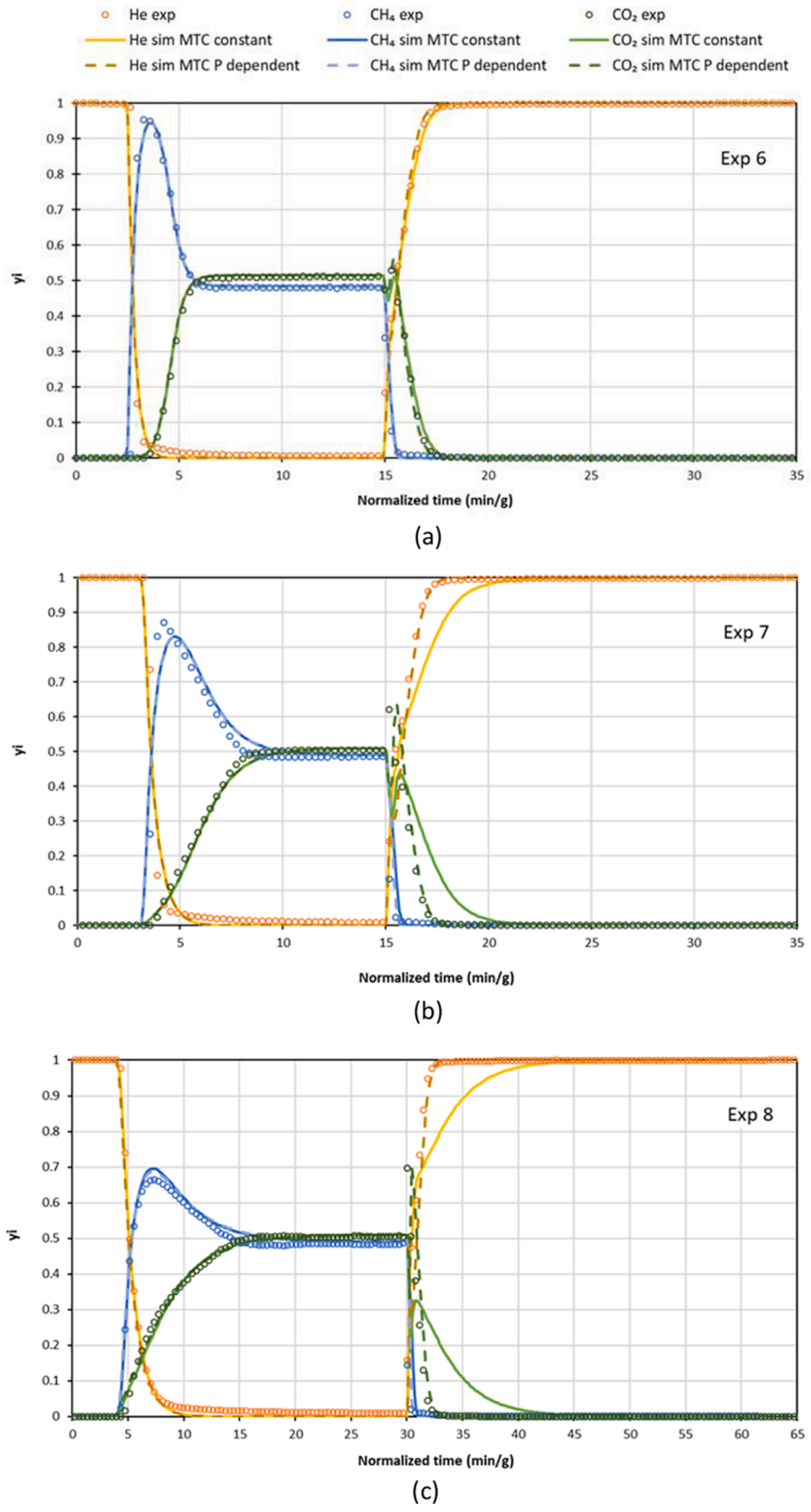

Fig. 3. Comparison between simulation results with a constant MTC (solid lines) or a pressure-dependent Arrhenius MTC (dash lines). Experimental results (symbols) for PSA cycles at an adsorption pressure of (a) 3 bar, (b) 5 bar, and (c) 10 bar.

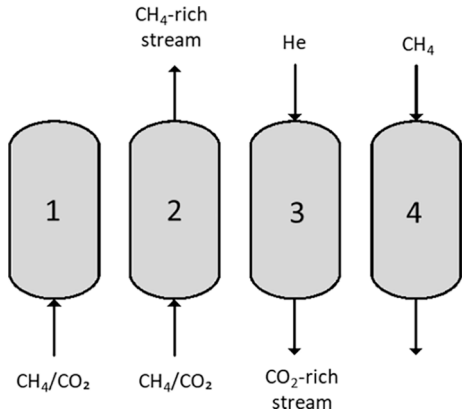

Fig. 4. Scheme of the 4-step counter-current PSA design used as the reference case for the CH_4-CO_2 separation: (1) pressurization with feed; (2) feed; (3) counter-current blowdown; (4) counter-current purge with pure methane.

Table 6
Conditions of the four-step PSA reference case configuration.

	Pressure (bar)	Temperature (°C)	Feed flow (mL/min)			Time (min)
			He	CH_4	CO_2	
Pressurization	1 → 3	30	0	15	15	1.5
Adsorption	3	30	0	15	15	12.5
Regeneration	1	30	50	0	0	7
Purge with CH_4	1	30	0	10	0	7

$$CO_2\ recovery = \frac{mol\ CO_2\ in\ raffinate}{total\ mol\ CO_2\ fed\ in\ cycle\ time} = \frac{\int_{t_A}^{t_B} F_{CO_2 out}\, dt}{\int_0^{t_A} F_{CO_2 in}\, dt} \quad (9)$$

In Eqs. (5) to (9), t_A refers to the time of the cycle at which the adsorption step ends, t_B refers to the time at which the blowdown step is finalized, and t_{Pu} to the end time of the purge with product step.$F_{CH_4 in}$ and $F_{CO_2 in}$ are the molar flow rates of CH_4 and CO_2, respectively, in the feed stream, while $F_{CH_4 out}$ and $F_{CO_2 out}$ are the molar flow rates leaving the adsorber. $m_{adsorbent}$ is the mass of adsorbent packed inside the column and t_{cycle} is the total duration of the cycle. Helium present in the product flow was not taken into account for the calculations, as it is an inert gas.

Table 6 summarizes the pressure, temperature, flow rate, and duration of the four steps of the reference case cycle configuration. A comprehensive analysis of the effect of the process parameters was pursued on this configuration by changing one parameter at a time.

In this base case analysis, the feed gas consisted of 30 mL/min of a 50:50 vol% CH_4-CO_2 gas mixture. The CO_2/CH_4 separation was carried out at an adsorption pressure of 3 bar. As previously commented, it was observed in the breakthrough experiments that a 3 bar time gap between both gases facilitates the separation. Besides, although the CO_2 and CH_4 adsorption capacities increased with pressure, the separation factor decreased. Therefore, 3 bar was selected as a compromise pressure.

The counter-current regeneration step was conducted at 1.2 bar with a helium flow of 50 mL/min, whereas 10 mL/min of CH_4 were employed during the purge step, counter-currently to the adsorption step.

In this case study, the schedule of the cycle defined equal durations of the adsorption (pressurization plus adsorption steps) and desorption (including regeneration and purge steps) to simulate the operation with two columns and to process the feed gas continuously; while the feed gas flows up through one bed the other is at regeneration. Hence, the total cycle time was 28 min.

The profiles of the molar flow rates of the different gas components in the exit stream over the cycle time are shown in Fig. 5. The four steps are labeled: pressurization (P), adsorption (A), blowdown (B) and purge with CH_4 (Pu).

During the pressurization step, there is no gas flow at the exit of the column. In the adsorption stage, a product stream of CH_4 at a high purity is obtained. The outlet CO_2 flow at this stage is negligible due to the preferential adsorption of CO_2 on the bed of activated carbon. Besides, the adsorption step ends before CO_2 breaks through the column. When the bed pressure blows down, a peak in the flow rate appears and both the CO_2 and CH_4 desorbed from the adsorbent bed. During the last step of the cycle, purge with methane, there is no product flow. All the pure methane of the feed is retained in the bed.

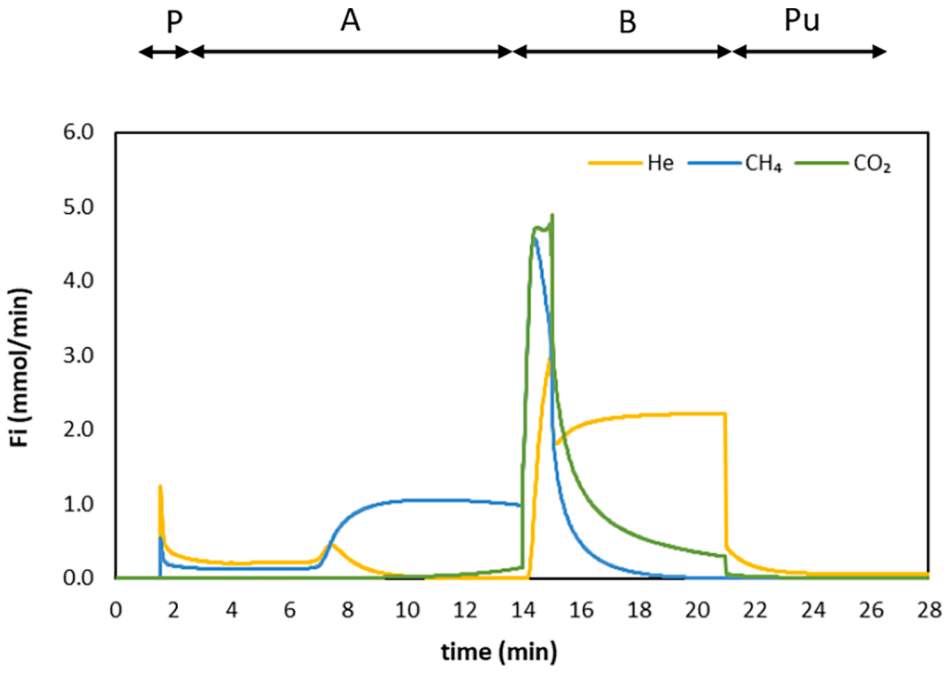

Fig. 5. Simulated molar flow rate profiles (He (yellow), CH_4 (blue) and CO_2 (green)) at the bed exit for the PSA reference case configuration.

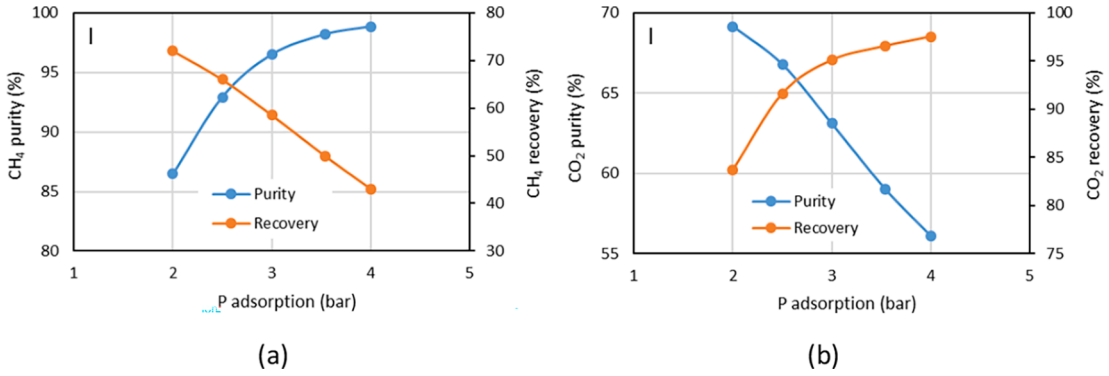

Fig. 6. Effect of the adsorption pressure on (a) the CH_4 purity and recovery, and (b) the CO_2 purity and recovery.

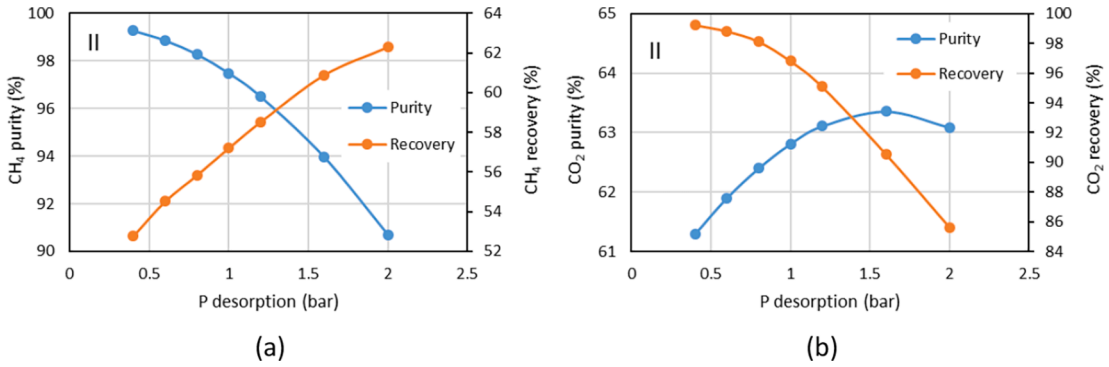

Fig. 7. Effect of the desorption pressure during blowdown on (a) the CH_4 purity and recovery, and (b) the CO_2 purity and recovery.

4.1. Parametric analysis of PSA configurations

This section analyzes the effect of the adsorption pressure, the regeneration conditions (i.e., desorption pressure, inert gas flow rate, purge flow rate), and the direction of the flow on the outcome of the simulated PSA cycles. The key indicators of the cyclic performance, i.e., CO_2 and CH_4 purity and recovery, were estimated once the cyclic steady-state was achieved. The reference case was the basis to run the sensitivity analysis by changing one parameter at a time.

I. Effect of the adsorption pressure

The influence of the adsorption pressure was assessed by varying it between 2 and 4 bar in different simulation cases. The duration of the pressurization and depressurization steps was assumed constant in all the simulations, independently of the pressure set point. On the other hand, the same k_{OP} value for CO_2 and CH_4 was used in all the cases (i.e., 10.5 and 158.6 bar/s, respectively, the values estimated for the 3 bar experiment). Fig. 6 plots the variation of the characteristic parameters with the adsorption pressure.

At higher adsorption pressures the CH_4 purity reaches a maximum due to the enhanced adsorption of CO_2; conversely, the recovery of methane drops down linearly with the adsorption pressure (Fig. 6a). CH_4 purity values range from 86.5% to 98.8% for the simulations at 2 and 4 bar, respectively. At an adsorption pressure of 3 bar, the average purity of the methane produced during the adsorption step is 96.5%, alongside a recovery of 58.5%. However, if the purity calculation only considered the first 10.5 min of this step, the CH_4 purity would achieve 99.1%.

As may be expected, the opposite trend is observed in the pattern of CO_2 purity and recovery (Fig. 6b). The CO_2 purity presents an inverse linear relationship with the adsorption pressure. The maximum value of the CO_2 purity (69.1%) is reached at 2 bar, whereas the highest CO_2 recovery (97.5%) corresponds to the experiment at 4 bar.

II. Effect of the desorption pressure

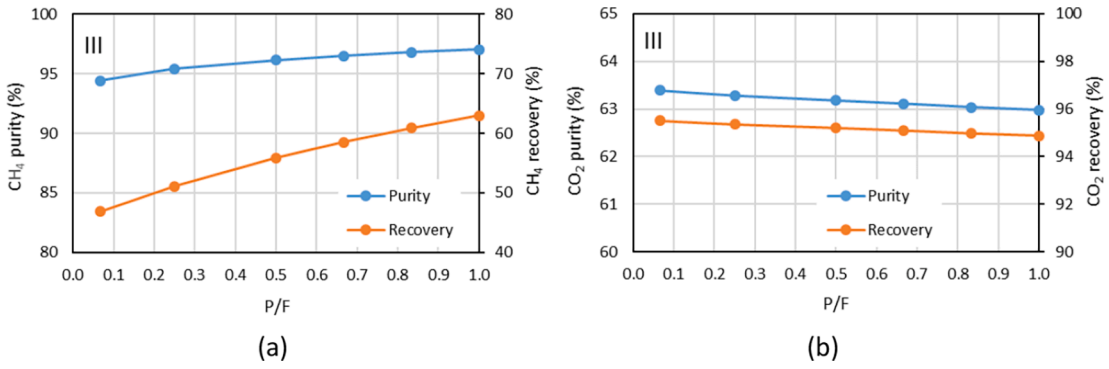

Fig. 8. Effect of the methane purge flow rate on (a) the CH_4 purity and recovery, and (b) the CO_2 purity and recovery.

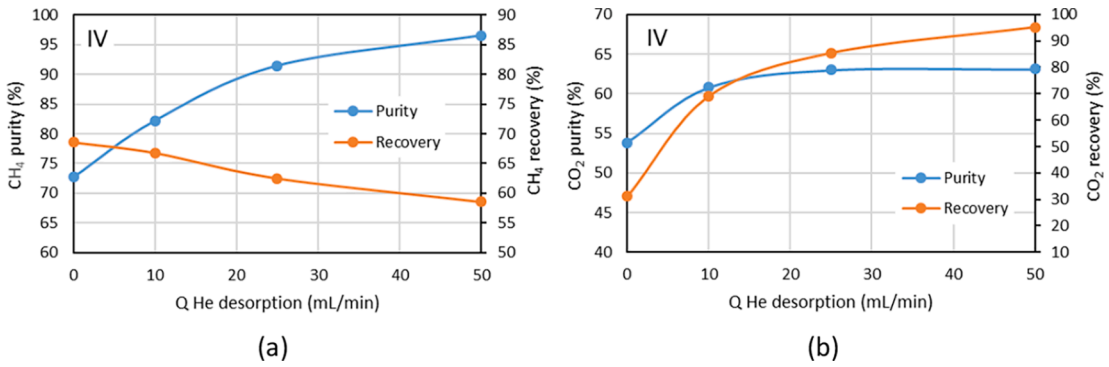

Fig. 9. Effect of the inert gas flow on (a) the CH_4 purity and recovery, and (b) CO_2 purity and recovery.

Different pressures between 0.4 bar and 2 bar were set during the regeneration stage to assess the influence of the desorption pressure on the process performance parameters. Simulation results are illustrated in Fig. 7.

Fig. 7 (a) and (b) show opposite trends on the CH_4 and CO_2 recovery for different desorption pressures. As may be expected, CO_2 recovery increases when the pressure is low. It is because of better regeneration of the adsorbent under these conditions. However, it should be recalled that the higher the vacuum level, the more the energy demand of the system. CO_2 purity seems to reach a maximum value (63.4%) at around 1.6 bar.

Concerning CH_4, a lower pressure during the blowdown step results in greater CH_4 purity in the product stream (99.3%). A lower pressure enhances the regeneration of the bed and substantially reduces the presence of CO_2 in the product stream. Nevertheless, the CH_4 recovery during the adsorption step also diminishes.

III. Effect of the purge flow rate

Different P/F ratios, defined as the quotient of the molar flows of CH_4 in the purge step and the biogas feed stream, were examined in this section. In the reference case configuration (see Table 6), the P/F ratio was set at 0.67 for a methane flow rate of 10 mL/min during the purge stage. Then, CH_4 purge flow rates between 1 and 15 mL/min were selected for the analysis, so the P/F ranged between 0.067 and 1. Fig. 8 shows the effect of the purge flow rate on the purity and recovery of both gas components.

Both the product purity and recovery follow similar upward trends and the best results correspond to the PSA configuration with the highest purge flow rate. The rise in the P/F ratio (from 0.067 to 1) increases the product (CH_4) purity and recovery, from 94.4% to 97.1% and from 46.9% to 63.0%, respectively. Nevertheless, it also means that a large amount of product (methane) is consumed in this step.

In Fig. 8b, it is observed that the variation of the purge to feed ratio has a minor effect on the CO_2 purity and recovery. Both parameters remain practically constant with the P/F ratio, showing a slight decrease as the flow rate of CH_4 increases.

IV. Effect of the inert gas flow rate

A series of simulation runs were conducted using different helium flow rates during the regeneration step but keeping all the other parameters fixed. The results are presented in Fig. 9.

Again CH_4 purity and recovery show opposite trends. The highest methane purity (96.5%) is reached for the highest inert gas flow rate (50 mL/min). When there is no inert gas fed during the regeneration step, the purity drops considerably (72.7%). Fig. 9a shows that the recovery of CH_4 during the adsorption stage, in which methane is the high purity product, is low at higher flow rates of He. However, the total gas recovery will increase given that the inert gas fed during regeneration helps to sweep the adsorbed gas components on the bed.

Regarding the CO_2 purity, the steepest increase (from 53.8 to 60.8%) happens in the range between feeding no inert gas and introducing a small flow rate (10 mL/min). Beyond this point, an increase in the flow rate of He has a negligible effect on the CO_2 purity. A similar trend applies to the CO_2 recovery, but in this case, the maximum value (95.1%) is reached for a helium flow rate of 50 mL/min.

V. Effect of the desorption time

The duration of the regeneration step was varied between 7 and 21 min. Consequently, the total cycle time changed accordingly, although the timing of the other stages remained. To keep a continuous feed of biogas to the process, the number of columns must increase from 2 to, at least, 3.

Fig. 10 shows that extending the desorption time from the base case (7 min) to 14 min results in a significant increase in the CO_2 recovery (from 95.1% to 99.4%). It also considerably enhances the CH_4 purity

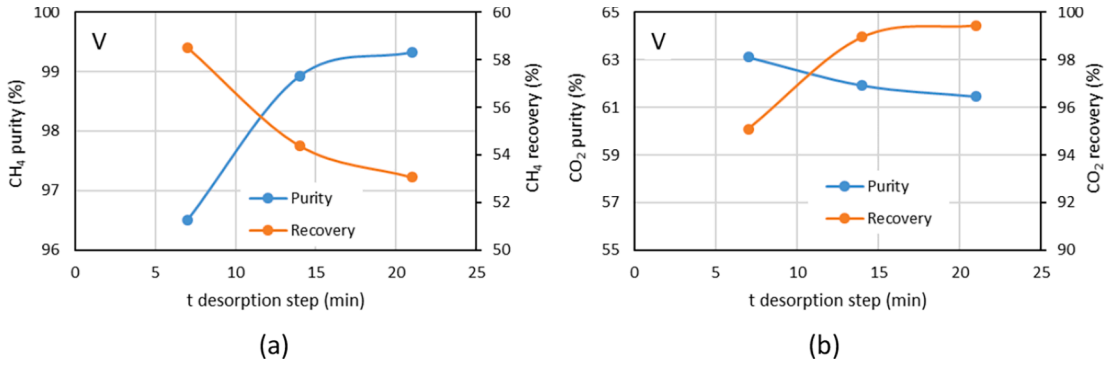

Fig. 10. Effect of the desorption time on (a) the CH_4 purity and recovery, and (b) the CO_2 purity and recovery.

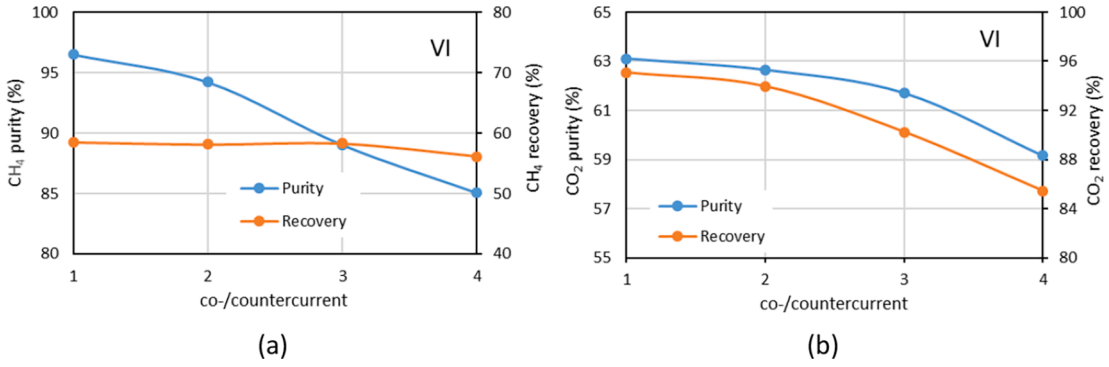

Fig. 11. Effect of the direction of the flow on (a) the CH_4 purity and recovery, and (b) the CO_2 purity and recovery.

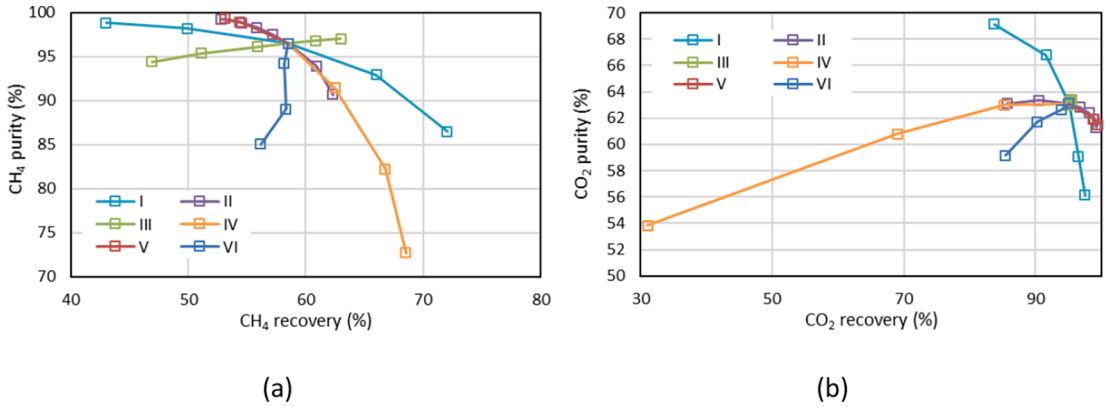

Fig. 12. Comparison of the performance of all the configurations simulated: (a) CH_4 purity *vs.* CH_4 recovery and (b) CO_2 purity *vs.* CO_2 recovery. The roman numbering corresponds to the cycle parameters analyzed in the previous section.

from 96.5% to 98.9%.

The efficiency of the regeneration step affects the amount of adsorbate remaining in the bed at the beginning of the next adsorption step. It is strongly dependent on the selected regeneration conditions such as the desorption pressure, step duration, and inert gas flow rate.

VI. Effect of the direction of the flow

The influence of the flow direction, co- or counter-currently to the biogas feed flow, was analyzed in this section to complete the sensitivity analysis. The parameters obtained for the reference case, where both the blowdown and purge steps proceeded counter-currently to the feed stream, were compared to other configurations performing the depressurization and/or the purge co-currently. The results are displayed in Fig. 11, where 1 = both counter-current; 2 = blowdown counter-current, purge co-current; 3 = blowdown co-current, purge counter-current; 4 = both co-current.

The process performance improves when both steps (regeneration and purge) run counter-currently to the feed flow direction. Both the CH_4 purity and the CO_2 purity and recovery reach their maximum values with this configuration.

When switching from performing all the steps in the same flow direction to conducting regeneration and purge stages counter-currently, the CO_2 purity increases from 59.2% to 63.1%, whereas the CO_2 recovery presents a sharp increase from 85.45 to 95.1%. The purity of methane also improves significantly (85.1% *vs.* 96.5%).

However, the gas flow direction in the different stages has very little influence on methane recovery, and simulations show similar values for all the studied configurations (see Fig. 11a).

4.2. Critical assessment of the PSA simulations

A critical assessment of all the cyclic configurations simulated in the previous section is conducted by representing the performance curve (plot of the purity *vs.* the recovery) for both gas components (CH_4 and CO_2) in Fig. 12.

The biogas upgrading process aims to achieve both high product (CH_4) purity and recovery. As previously observed, both parameters tend to show opposite trends with the cycle parameters. Therefore, it is usually necessary to reach a compromise when selecting the optimum cyclic configuration. It will also depend on the requirements of the foreseen application of the CO_2/CH_4 separation process.

Looking at Fig. 12a it is possible to conclude that for a 4-stage PSA cycle, a CH_4 rich-stream with a purity higher than 95% and a recovery of around 60% can be achieved in configurations where a higher P/F ratio is employed (P/F value between 0.67 and 1). Furthermore, the optimum adsorption pressure value is around 3 bar while desorption should be performed at slightly higher values than atmospheric pressure (between 1.2 and 1.6 bar).

Another characteristic parameter in the assessment of PSA cycles is the product productivity (in this case, methane). The productivity of the adsorbent accounts for the moles of product produced per mass of adsorbent and per unit time. Therefore, the CH_4 recovery and cycle time directly impact productivity values. Fig. 13 summarizes the estimated productivity values for the simulated configurations.

According to the values reported in Fig. 13, the CH_4 productivity is mainly influenced by the adsorption pressure, desorption time, and P/F ratio selected in the simulations. The highest productivity (4.8 mol/kg•h) was reached for the PSA cycle conducted at an adsorption pressure of 2 bar (Fig. 13a), followed by the simulation employing 15 mL/min of CH_4 during the purge step (P/F = 1 in Fig. 13c). The configuration

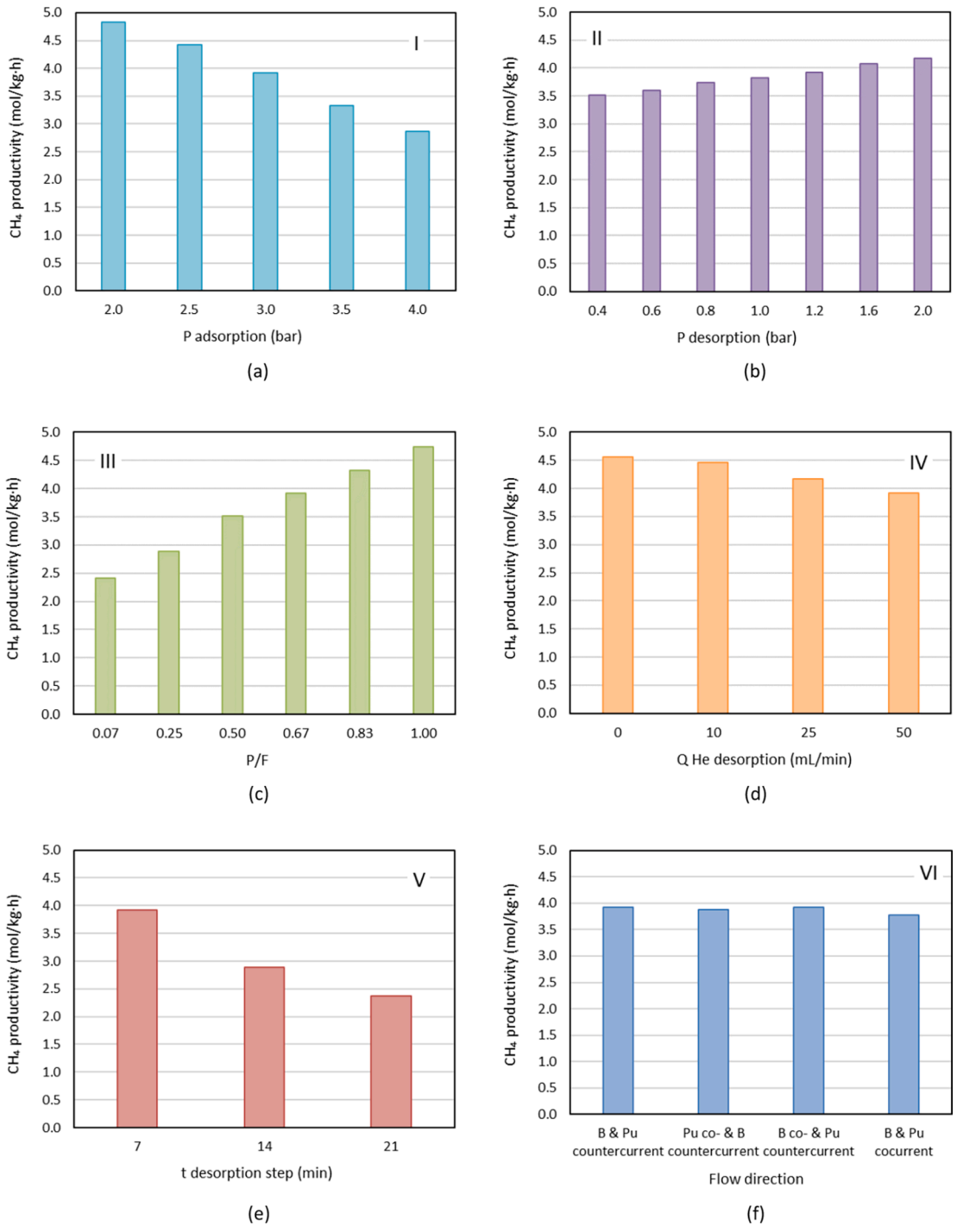

Fig. 13. CH_4 productivity (mol/kg•h) for the simulated PSA configurations.

without sweeping inert gas during the regeneration stage (see Fig. 13d) also results in high CH_4 productivity at the expense of the lowest CH_4 purity of all the configurations simulated.

The evolution of the CH_4 productivity with the desorption pressure is plotted in Fig. 13b and ranges from 3.5 to 4.2 mol/kg•h. A decreasing tendency can be observed as the pressure used during the regeneration diminishes. However, lower pressures during regeneration enhance the amount of CH_4 recovered at this stage rather than during the adsorption stage. It should be noted that the CH_4 productivity is calculated in the product stream exiting the bed during the adsorption step since it presents greater CH_4 purity which explains the lower productivity values.

The lowest productivity corresponded to the configuration with a regeneration step of 21 min (see Fig. 13e). It stems from the longer total cycle time which, in turn, reduces the amount of CH_4 obtained per unit of time. On the other hand, flow direction has practically no effect on the production values, as observed in Fig. 13f.

4.3. *Scale-up of the PSA process*

A preliminary scale-up of the PSA process evaluated above was proposed. Simulations run on a column with a height of 50 cm and 5.5 cm inner diameter, assuming the same bed density as in the fixed-bed lab set-up. The column was then packed with approximately 300 g of adsorbent, which is 75 times higher than the mass experimentally tested.

Table 7
Results obtained for the simulation of scaling-up the adsorption column.

	V = 15.7 cm^3	V = 1180.4 cm^3 Case A (same v_s)	Case B (same t_b CO_2)
CH_4 purity (vol.% CH_4)	96.5	98.0	96.9
CH_4 recovery (vol.% CH_4)	58.5	66.7	62.2
CO_2 recovery (vol.% CO_2)	63.1	68.5	65.2
CO_2 purity (vol.% CO_2)	95.1	96.5	94.9
Productivity (mol/kg•h)	3.9	1.0	3.7

A 4-step 2-bed configuration was simulated with this scaled-up column, testing two different total flow rates. Firstly, in Case A, a surface velocity equal to the reference case (Table 6) that implied longer times to achieve the saturation of the bed (the total cycle time was 116 min). In the second, Case B, a total flow rate of 2050 mL/min fed the column during the adsorption step obtaining a similar breakthrough time for CO_2 as in the reference case. The timing of the cycle steps was also maintained.

The characteristic parameters of the scaled-up PSA cyclic configurations are compared in Table 7 with the simulation of the experimental bed.

Increasing the scale of the bed improved CH_4 and CO_2 purity and recovery. It is only in Case B that a slightly lower purity of CO_2 was attained. However, the productivity diminished quite significantly in Case A due to a much longer cycle time.

5. Conclusions

A biogas upgrading PSA process with biomass-based activated carbon has been studied. Breakthrough curves simulations were obtained by solving a mathematical model developed with Aspen Adsorption™ that describes the adsorption equilibrium and kinetics. Mass transfer coefficients for CO_2 and CH_4 were estimated by fitting the simulated curves to the experimental results.

The dynamic model predicted with high accuracy the breakthrough times and adsorption capacities for CH_4 and CO_2, although light discrepancy was observed in the experiments where adsorption occurred at 5 and 10 bar. On the other hand, applying pressure-dependent mass transfer coefficients in the PSA cycles at higher adsorption pressures showed improved results due to it influencing the desorption rate.

Skarstrom-type four-step cycles were designed based on the dynamic model validated with the experimental results. Sensitivity analysis was conducted based on the estimates of key performance parameters to identify the optimum cyclic configuration. Most PSA simulations resulted in a product purity above 90% that could reach values above 97% when considering only the first 10.5 min of the adsorption stage. Depending on the country's regulations, the CO_2 content for pipeline-grade biomethane should be below 2–3% [54]. Therefore, the produced biomethane would meet the requirements for injection to the gas grid.

Both the use of higher methane purge and inert gas flow rates during the regeneration step improved CH_4 purity. The extended regeneration step, enhanced CH_4 purity (99.3%) but negatively impacted the adsorbent productivity (2.4 mol/kg•h). A CH_4 purity of 99.3% could also be reached when applying light vacuum for desorption at 0.4 bar, at the expense of increase the energy consumption. Discrete values of CH_4 recovery were obtained, between 43% and 72.1%, for the simulation runs at adsorption pressures of 4 and 2 bar, respectively. Finally, it was shown that conducting counter-current blowdown and purge is beneficial regarding CH_4 and CO_2 purity and recovery but did not affect CH_4 productivity.

Hence, it is feasible to develop a PSA process for CO_2/CH_4 separation using environmentally sustainable, low-cost adsorbent material. A trade-off needs to be considered between CH_4 purity, recovery and productivity when designing a biogas upgrading PSA process. Future research should focus on the effect of adding pressurization steps to enhance process performance or assessing other components, such as water vapor, in the biogas stream.

Declaration of Competing Interest

The authors declare that they have no known competing financial interests or personal relationships that could have appeared to influence the work reported in this paper.

Acknowledgements

This work was carried out with financial support from the Gobierno del Principado de Asturias (PCTI, Ref. IDI/2018/000115), co-financed by the European Regional Development Fund (ERDF), and from the CSIC (Project PIE, Ref. 202080E115).

Appendix A. Supplementary data

Supplementary data to this article can be found online at https://doi.org/10.1016/j.cej.2021.132564.

References

[1] I. Durán, N. Álvarez-Gutiérrez, F. Rubiera, C. Pevida, Biogas purification by means of adsorption on pine sawdust-based activated carbon: impact of water vapor, Chem Eng J 353 (2018) 197–207.
[2] F. Bauer, T. Persson, C. Hulteberg, D. Tamm, Biogas upgrading - technology overview, comparison and perspectives for the future, Biofuels, Bioprod Biorefining 7 (5) (2013) 499–511.
[3] I. Angelidaki, L. Treu, P. Tsapekos, G. Luo, S. Campanaro, H. Wenzel, P.G. Kougias, Biogas upgrading and utilization: current status and perspectives, Biotechnol Adv 36 (2) (2018) 452–466.
[4] A.I. Adnan, M.Y. Ong, S. Nomanbhay, K.W. Chew, P.L. Show, Technologies for Biogas Upgrading to Biomethane: a Review, Bioengineering 6 (4) (2019) 92.
[5] E. Ryckebosch, M. Drouillon, H. Vervaeren, Techniques for transformation of biogas to biomethane, Biomass Bioenergy 35 (5) (2011) 1633–1645.
[6] C. Grande, Biogas upgrading by pressure swing adsorption, In: Biofuel's Eng. Process Technol. (2011).
[7] A. Mersmann, B. Fill, R. Hartmann, S. Maurer, The potential of energy saving by gas-phase adsorption processes, Chem Eng Technol 23 (11) (2000) 937–944.
[8] G. Hofer, J. Fuchs, G. Schöny, T. Pröll, Heat transfer challenge and design evaluation for a multi-stage temperature swing adsorption process, Powder Technol 316 (2017) 512–518.
[9] Skarstrom CW. Method and apparatus for fractionating gaseous mixtures by adsorption, U.S. patent no. 2944627. 1960.
[10] M. Asgari, H. Anisi, H. Mohammadi, S. Sadighi, Designing a commercial scale Pressure Swing Adsorber for Hydrogen, purification. 56 (5) (2014) 552–561.
[11] M. Yáñez, F. Relvas, A. Ortiz, D. Gorri, A. Mendes, I. Ortiz, PSA purification of waste hydrogen from ammonia plants to fuel cell grade, Sep Purif Technol 240 (2020) 116334, https://doi.org/10.1016/j.seppur.2019.116334.
[12] L. Riboldi, O. Bolland, Overview on pressure swing adsorption (PSA) as CO_2 capture technology: state-of-the-art, Limits and Potentials. Energy Procedia 114 (114) (2017) 2390–2400.
[13] R.T. Yang, Gas Separation by Adsorption Processes, Butterworth, 1987.
[14] D. Ruthven, S. Farooq, K. Knaebel, Pressure Swing Adsorption, VCH Publishers, 1994.
[15] L.A.M. Rocha, K.A. Andreassen, C.A. Grande, Separation of CO_2/CH_4 using carbon molecular sieve (CMS) at low and high pressure, Chem Eng Sci 164 (2017) 148–157.
[16] C.A. Grande, R. Blom, A. Möller, J. Möllmer, High-pressure separation of CH_4/CO_2 using activated carbon, Chem Eng Sci 89 (2013) 10–20.
[17] D. Peredo-Mancilla, C. Matei Ghimbeu, B.N. Ho, M. Jeguirim, C. Hort, D. Bessieres, Comparative study of the CH_4/CO_2 adsorption selectivity of activated carbons for biogas upgrading, J Environ Chem Eng 7 (5) (2019).
[18] M.V. Gil, N. Álvarez-Gutiérrez, M. Martínez, F. Rubiera, C. Pevida, A. Morán, Carbon adsorbents for CO_2 capture from bio-hydrogen and biogas streams: breakthrough adsorption study, Chem Eng J 269 (2015) 148–158.
[19] P.C. Vilella, J.A. Lira, D.C.S. Azevedo, M. Bastos-Neto, R. Stefanutti, Preparation of biomass-based activated carbons and their evaluation for biogas upgrading purposes, Ind Crops Prod 109 (2017) 134–140.
[20] M.J. Prauchner, S. da C Oliveira, F. Rodríguez-Reinoso, Tailoring low-cost granular activated carbons Intended for CO_2 adsorption, Front Chem 8 (November) (2020) 1–16.

[21] M. Bernardo, N. Lapa, I. Fonseca, I.A.A.C. Esteves, Biomass valorization to produce porous carbons: applications in CO_2 capture and biogas upgrading to biomethane—A mini-review, Front Energy Res 9 (March) (2021) 1–6.
[22] Z. Bacsik, O. Cheung, P. Vasiliev, N. Hedin, Selective separation of CO_2 and CH_4 for biogas upgrading on zeolite NaKA and SAPO-56, Appl Energy 162 (2016) 613–621.
[23] C.A. Grande, A.E. Rodrigues, Biogas to fuel by vacuum pressure swing adsorption I, Behavior of Equilibrium and Kinetic-Based Adsorbents. 46 (13) (2007) 4595–4605.
[24] Arya A, Divekar S, Rawat R, Gupta P, Garg MO, Dasgupta S, et al. Upgrading Biogas at Low Pressure by Vacuum Swing Adsorption.
[25] S. Cavenati, C.A. Grande, A.E. Rodrigues, C. Kiener, U. Müller, Metal organic framework adsorbent for biogas upgrading, Ind Eng Chem Res 47 (16) (2008) 6333–6335.
[26] L. Hamon, N. Heymans, P.L. Llewellyn, V. Guillerm, A. Ghoufi, S. Vaesen, et al., Separation of CO_2–CH_4 mixtures in the mesoporous MIL-100(Cr) MOF: experimental and modelling approaches, Dalt Trans 41 (14) (2012) 4052.
[27] A.F.P. Ferreira, A.M. Ribeiro, S. Kulaç, A.E. Rodrigues, Methane purification by adsorptive processes on MIL-53(Al), Chem Eng Sci 124 (2015) 79–95.
[28] A. Khan, M.A. Qyyum, H. Saulat, R. Ahmad, X.S. Peng, M. Lee, Metal–organic frameworks for biogas upgrading: recent advancements, challenges, and future recommendations, Appl Mater Today 22 (2021) 100925.
[29] M.S. Shafeeyan, W.M.A. Wan Daud, A. Shamiri, A review of mathematical modeling of fixed-bed columns for carbon dioxide adsorption, Chem. Eng. Res. Des. 92 (5) (2014) 961–988.
[30] A. Kapoor, R.T. Yang, Kinetic separation of methane-carbon dioxide mixture by adsorption on molecular sieve carbon, Chem Eng Sci 44 (8) (1989) 1723–1733.
[31] S. Cavenati, C.A. Grande, A.E. Rodrigues, Upgrade of methane from landfill gas by pressure swing adsorption, Energy Fuels 19 (6) (2005) 2545–2555.
[32] M.B. Kim, Y.S. Bae, D.K. Choi, C.H. Lee, Kinetic separation of landfill gas by a two-bed pressure swing adsorption process packed with carbon molecular sieve: nonisothermal operation, Ind Eng Chem Res 45 (14) (2006) 5050–5058.
[33] Y.J. Kim, Y.S. Nam, Y.T. Kang, Study on a numerical model and PSA (pressure swing adsorption) process experiment for CH_4/CO_2 separation from biogas, Energy 91 (2015) 732–741.
[34] R. Augelletti, M. Conti, M.C. Annesini, Pressure swing adsorption for biogas upgrading. a new process configuration for the separation of biomethane and carbon dioxide, J Clean Prod 140 (2017) 1390–1398.
[35] R.L.S. Canevesi, K.A. Andreassen, E.A. da Silva, C.E. Borba, C.A. Grande, Pressure swing adsorption for biogas upgrading with carbon molecular sieve, Ind Eng Chem Res 57 (23) (2018) 8057–8067.
[36] M.P.S. Santos, C.A. Grande, A.E. Rodrigues, Pressure swing adsorption for biogas upgrading. effect of recycling streams in pressure swing adsorption design, Ind Eng Chem Res 50 (2) (2011) 974–985.
[37] Y. Shen, W. Shi, D. Zhang, P. Na, B. Fu, The removal and capture of CO_2 from biogas by vacuum pressure swing process using silica gel, J CO2 Util 27 (July) (2018) 259–271.
[38] G. Singh, K.S. Lakhi, S. Sil, S.V. Bhosale, I.Y. Kim, K. Albahily, et al., Biomass derived porous carbon for CO_2 capture, Carbon N Y 148 (2019) 164–186.
[39] G.G. Stavropoulos, A.A. Zabaniotou, Minimizing activated carbons production cost, Fuel Process Technol 90 (7-8) (2009) 952–957.
[40] H. Gu, R. Bergman, N. Anderson, S. Alanya-Rosenbaum, Life cycle assessment of activated carbon from woody biomass, Wood Fiber Sci 50 (3) (2018) 229–243.
[41] I.M. Lima, A. McAloon, A.A. Boateng, Activated carbon from broiler litter: process description and cost of production, Biomass Bioenergy 32 (6) (2008) 568–572.
[42] K. Bonnot, D. Tondeur, L. Luo, Effects of composition, temperature and purge on the performance of the cyclic adsorption of CO_2 and CH_4 on activated carbon, Chem Eng Res Des 84 (3A) (2006) 192–208.
[43] F. Foeth, M. Andersson, H. Bosch, G. Aly, T. Reith, Separation of dilute CO_2-CH_4 mixtures by adsorption on activated carbon, Sep Sci Technol 29 (1) (1994) 93–118.
[44] B. Wu, X. Zhang, Y. Xu, D. Bao, S. Zhang, Assessment of the energy consumption of the biogas upgrading process with pressure swing adsorption using novel adsorbents, J Clean Prod 101 (2015) 251–261.
[45] M.G. Plaza, I. Durán, F. Rubiera, C. Pevida, CO_2 adsorbent pellets produced from pine sawdust: effect of coal tar pitch addition, Appl Energy 144 (2015) 182–192.
[46] C.A. Grande, A.E. Rodrigues, Layered vacuum pressure-swing adsorption for biogas upgrading, Ind Eng Chem Res 46 (23) (2007) 7844–7848.
[47] D. Leinekugel-le-Cocq, M. Tayakout-Fayolle, Y. Le Gorrec, C. Jallut, A double linear driving force approximation for non-isothermal mass transfer modeling through bi-disperse adsorbents, Chem Eng Sci 62 (15) (2007) 4040–4053.
[48] J. Park, J.W. Lee, Dynamic modeling of fixed-bed adsorption of flue gas using a variable mass transfer model, Korean J Chem Eng 33 (2) (2016) 438–447.
[49] R.H. Kang, J. Park, D. Kang, J.W. Lee, Evaluating isotherm models for the prediction of flue gas adsorption equilibrium and dynamics, Korean J Chem Eng 35 (3) (2018) 734–743.
[50] K.S. Hwang, W.K. Lee, The adsorption and desorption breakthrough behavior of carbon monoxide and carbon dioxide on activated carbon. effect of total pressure and pressure-dependent mass transfer coefficients, Sep Sci Technol 29 (14) (1994) 1857–1891.
[51] N.S. Raghavan, M.M. Hassan, D.M. Ruthven, Numerical simulation of a PSA system. part I: isothermal trace component system with linear equilibrium and finite mass transfer resistance, AIChE J 31 (3) (1985) 385–392.
[52] K.J. Sladek, E.R. Gilliland, R.F. Baddour, K.J. Sladek, Diffusion on surfaces. II. correlation of diffusivities of physically and chemically adsorbed species, Ind Eng Chem Fundam 13 (2) (1974) 100–105.
[53] S. García, M.V. Gil, C.F. Martín, J.J. Pis, F. Rubiera, C. Pevida, et al., Breakthrough adsorption study of a commercial activated carbon for pre-combustion CO_2 capture, Chem Eng J 171 (2) (2011) 1–25.
[54] O.W. Awe, Y. Zhao, A. Nzihou, D.P. Minh, N. Lyczko, A review of biogas utilisation, purification and upgrading technologies, Waste Biomass Valorization 8 (2) (2017) 267–283.